

Topological electronic structure and Weyl semimetal in the TlBiSe_2 class of semiconductors

Bahadur Singh¹, Ashutosh Sharma¹, H. Lin², M.Z. Hasan^{3,4}, R. Prasad¹ and A. Bansil²

¹*Department of Physics, Indian Institute of Technology Kanpur, Kanpur 208016, India*

²*Department of Physics, Northeastern University, Boston, Massachusetts 02115, USA*

³*Joseph Henry Laboratory, Department of Physics,*

Princeton University, Princeton, New Jersey 08544, USA

⁴*Princeton Center for Complex Materials, Princeton University, Princeton, New Jersey 08544, USA*

We present an analysis of bulk and surface electronic structures of thallium based ternary III-V-VI₂ series of compounds TIMQ_2 , where $\text{M}=\text{Bi}$ or Sb and $\text{Q}=\text{S}$, Se or Te , using the *ab initio* density functional theory framework. Based on parity analysis and (111) surface electronic structure, we predict TlSbSe_2 , TlSbTe_2 , TlBiSe_2 and TlBiTe_2 to be non-trivial topological insulators with a single Dirac cone at the Γ -point, and TlSbS_2 and TlBiS_2 to be trivial band insulators. Our predicted topological phases agree well with available angle-resolved photoemission spectroscopy (ARPES) measurements, in particular the topological phase changes between TlBiSe_2 and TlBiS_2 . Moreover, we propose that Weyl semimetal can be realized at the topological critical point in $\text{TlBi}(\text{S}_{1-x}\text{Se}_x)_2$ and $\text{TlBi}(\text{S}_{1-x}\text{Te}_x)_2$ alloys by breaking the inversion symmetry in the layer by layer growth in the order of $\text{Tl-Se}(\text{Te})\text{-Bi-S}$, yielding six Dirac cones centered along the $\Gamma-L$ directions in the bulk band structure.

PACS numbers: 71.20.Nr, 71.15.Dx, 71.10.Pm, 73.20.At

I. INTRODUCTION

Topological insulators are a new class of materials, which have attracted intense interest in the last few years¹⁻³ due to their exotic properties. These materials support an odd number of surface state bands with linear dispersion in the bulk energy gap, which can be viewed as a sea of massless Dirac Fermions. The conducting surface states in topological insulators are protected by time-reversal symmetry and are immune to scattering by non-magnetic impurities, thus opening new avenues for dissipationless transport. There also is a vigorous ongoing search for topological superconductors^{4,5}, with the possibility of realizing Majorana fermions, which are their own antiparticles⁶ with potential application to quantum computing⁷. Topological insulators have also generated a considerable excitement due to the possibility of exploring the *Higgs mechanism* and realization of a Weyl semimetal in a condensed matter system.⁸⁻¹³

A topological phase was initially predicted in 2D HgTe/CdTe quantum wells¹⁴ and subsequently verified experimentally¹⁵. Soon thereafter a 2D conducting surface state was realized in the bulk band gap of three dimensional thermoelectrics¹⁶⁻¹⁸ $\text{Bi}_{1-x}\text{Sb}_x$, Bi_2Se_3 , Bi_2Te_3 and Sb_2Te_3 . However, magnetotransport studies¹⁹⁻²¹ have shown that bulk transport dominates in these materials, motivating continued search for other 3D topological insulators with single Dirac cone surface states residing in the bulk energy gap. Since then first-principles calculations have suggested a large variety of topologically interesting materials ranging from oxides²² to the Heusler family of compounds²³⁻²⁵. Another class is thallium based ternary III-V-VI₂ chalcogenides, which were proposed theoretically^{26,27} and then verified experimentally²⁸⁻³⁰. These studies showed the existence

of single Dirac cone type surface states at the Γ -point in TlSbSe_2 , TlSbTe_2 , TlBiSe_2 and TlBiTe_2 . Also, it has been found that *p* doped TlBiTe_2 superconducts³¹, where superconductivity is attributed to six leaf like bulk pockets in the Fermi surface and the surface state becomes superconducting²⁹.

Interestingly, recent studies^{32,33} of $\text{TlBi}(\text{S}_{1-x}\text{Se}_x)_2$ alloys show that a topological phase transition can be realized by modulating either spin-orbit coupling or the crystal structure, and that the surface Dirac fermion becomes massive at the quantum phase transition. This can be viewed as a condensed matter version of the *Higgs mechanism* in which a particle acquires a mass by spontaneous symmetry breaking. This system thus may provide a model system which connects condensed-matter physics to particle physics. It has also been proposed that a Weyl semimetal phase^{34,35} could be achieved at the phase transition between a topological and normal insulator if we explicitly break time reversal symmetry^{8,9} or inversion symmetry^{10,11}. In this new phase, valence and conduction bands touch at certain points, called Weyl points, where dispersion is linear. These Weyl points come in pairs with positive and negative helicities and are robust to perturbations in the bulk material.

Our motivation for undertaking the present study is to provide a comprehensive investigation of the bulk and surface electronic structures of the thallium based ternary III-V-VI₂ series of compounds TIMQ_2 , where $\text{M}=\text{Bi}$ or Sb and $\text{Q}=\text{S}$, Se or Te , within a uniform first principles framework. In particular, not only the nontrivial compounds are studied^{36,37} but the topologically trivial compounds $\text{TlBi}(\text{Sb})\text{S}_2$ is included since the recent ARPES measurement observed the topological phase transition in the alloy $\text{TlBi}(\text{Se},\text{S})_2$ between nontrivial TlBiSe_2 and trivial TlBiS_2 .³³ We compare our

theoretical predictions with the available ARPES results. Insight into the topological nature of these compounds is gained through slab computations in which the thickness of the slab is varied. Finally, the possibility of realizing a Weyl semimetal phase through strain in $\text{TlBi}(\text{S}_{1-x}\text{Se}_x)_2$ and $\text{TlBi}(\text{S}_{1-x}\text{Te}_x)_2$ alloys is examined for the first time, and it is shown that, when the inversion symmetry of the system is broken, a Weyl phase is indeed possible at the topological critical point where the system undergoes a transition from a trivial to a non-trivial (topological) insulator. Bulk and surface electronic structures of many members of the six ordered TI-compounds considered in this work have been discussed in several earlier papers in the literature.^{26,27,36,37}

The organization this article is as follow. Section II gives details of the bulk and surface computations. In section III, we explain the bulk crystal structures, electronic structure and the parity analysis used to infer the topological nature of various compounds. Section IV discusses the slab structure used, relaxation and size dependent effects. In section V, we explain the topological phase transition and realization of the Weyl semimetal phase in $\text{TlBi}(\text{S}_{1-x}\text{Se}_x)_2$ and $\text{TlBi}(\text{S}_{1-x}\text{Te}_x)_2$ alloys. Section VI summarizes conclusions of this study.

II. COMPUTATIONAL DETAILS

Electronic structure calculations were carried out within the framework of the density functional theory³⁸ using VASP³⁹ (*Vienna ab initio Simulation Package*), with projected augmented wave basis⁴⁰. Exchange-correlation effects were treated using a generalized gradient approximation⁴¹ and the spin-orbit coupling (SOC) effects are included as implemented in the VASP package. For structure optimization a plane wave cut-off energy of 350 eV and a Γ -centered $8 \times 8 \times 8$ k-mesh with conjugate gradient algorithm (CGA)⁴² was used. Lattice parameters and ionic positions were adjusted until all components of Hellman-Feynman force on each ion were less than 0.001 eV/Å. Our surface electronic structure calculations are based on a slab geometry using bulk relaxed parameters with a net vacuum of 15 Å, a plane wave cut-off energy of 350 eV, and a Γ -centered $9 \times 9 \times 1$ k-mesh. Since ionic relaxations^{36,37} are important, ionic positions in all slabs were optimized until the z-component of the Hellman-Feynman forces was less than 0.005 eV/Å. Topological phase transition in $\text{TlBi}(\text{S}_{1-x}\text{Se}_x)_2$ and $\text{TlBi}(\text{S}_{1-x}\text{Te}_x)_2$ systems was investigated by taking the critical concentration of sulfur to be $x=0.5$ ³³.

III. RESULTS AND DISCUSSION

A. Bulk Crystal Structure

Thallium based ternary chalcogenides III-V-VI₂ share a rhombohedral crystal structure (space group D_{3d}^5 ($R\bar{3}$

m)) with four atoms per unit cell which occupy the Wyck-off positions 3a, 3b, and 6c⁴³. We illustrate the crystal structure with the example of TlBiTe_2 , which can be viewed as a distorted NaCl structure with four atoms in the primitive unit cell⁴³⁻⁴⁵ and a sequence of hexagonal close packed layers in the order Tl-Te-Bi-Te (see Fig.1). The conventional unit cell is hexagonal and contains 12

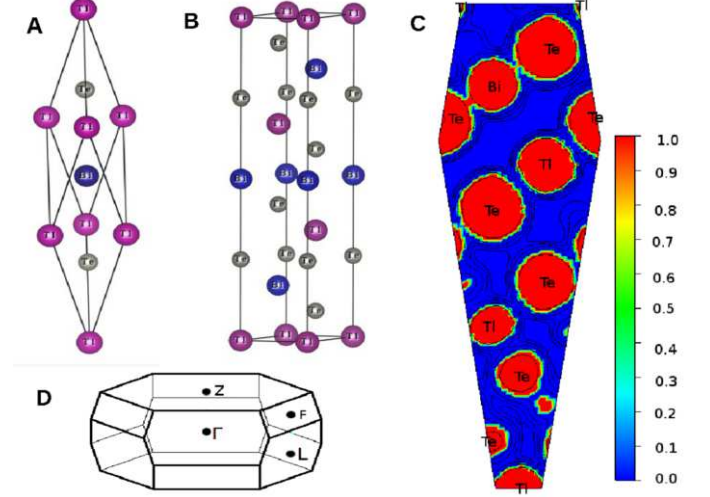


FIG. 1. Primitive (A) and conventional (B) hexagonal crystal structure for TlBiTe_2 . The conventional (hexagonal) unit cell has three times more atoms than primitive cell. (C) ELF plot of TlBiTe_2 (see text). (D) Brillouin zone for the primitive unit cell with four time reversal invariant points Γ , F, Z and L.

atoms. The hexagonal lattice constants a_H and c_H can be computed from the rhombohedral parameters via the relation

$$a_H = 2a_R \sin \frac{\alpha}{2}, \quad c_H = a_R \sqrt{3 + 6 \cos \alpha} \quad (1)$$

where a_R is the rhombohedral lattice constant and α is the rhombohedral angle. Notably, the present compounds form a layered structure similar to binary topological insulators A_2B_3 ($A=\text{Bi, Sb}$ and $B=\text{Se, Te}$)¹⁶ where atoms are arranged in a sequence of five atomic layers or a quintuple repeating pattern. The bonding within the quintuple of layers is ionic-covalent type while between one quintuple group and the next is van-der Waals type⁴⁶. In order to gain insight into the nature of bonding in the thallium based chalcogenides we have performed an ELF (Electron Localization Function)⁴⁷ study, which shows that there is a negligible value of the ELF between the thallium and tellurium layers, indicating predominantly ionic type bonding between these layers. In contrast, the value of ELF between the bismuth and tellurium layers is significant implying ionic-covalent type bonding. The optimized lattice and internal parameters u for the six TI-compounds considered are given in Table 1.

TABLE I. Optimized lattice constant a_R , angle α and internal parameter u for six thallium based rhombohedral compounds.

| Compound | a_R (Å) | α (degrees) | u |
|---------------------|--------------|-----------------------|--------|
| TlSbSe ₂ | 7.955 | 30.869 | 0.2374 |
| TlSbTe ₂ | 8.421 | 31.367 | 0.2386 |
| TlSbS ₂ | 7.718 | 30.568 | 0.2352 |
| TlBiSe ₂ | 7.989 | 31.368 | 0.2391 |
| TlBiTe ₂ | 8.367 | 31.847 | 0.2413 |
| TlBiS ₂ | 7.979 | 29.764 | 0.2368 |

B. Bulk Band Structures

The bulk band structures of TlSbQ₂ (Q=S, Se, and Te), shown in Fig 2, indicate these three compounds to be narrow gap semiconductors. TlSbSe₂ is seen to be a direct band gap semiconductor with the valence band maximum (VBM) and conduction band minimum (CBM) lying along $\Gamma - L$. Here the spin-orbit coupling plays an important role as it induces a band inversion at Γ suggesting a possible nontrivial topological phase, a point to which we return below. TlSbTe₂ and TlSbS₂ are also seen from Figs. 2(B)-(C) to be direct band gap semiconductors with VBM and CBM at the Γ -point. Since Te is heavier than Se, there is a large spin-orbit (SOC) effect in TlSbTe₂. But S atom is lighter than Se and Te so that SOC effects are smaller in TlSbS₂.

The bulk band structures of TlBiQ₂ (Q=Se, Te, and S) are shown in Fig.3. There is a large effect of spin-orbit coupling due to presence of the heavier Bi atom. Our band structures agree well with an earlier study⁴⁵, except in the case of TlBiTe₂, which was previously found to be⁴⁵ an indirect gap semiconductor with the VBM lying along the $L - Z$ direction and the CBM at the Γ -point. However, for our relaxed structure (including spin-orbit coupling) the VBM and CVM still lie at the aforementioned \vec{k} -points, but the system is semi-metallic with a band gap of -10 meV. This is in accord with the corresponding experimental results²⁹, which found the material to be semi-metallic with a band gap of -20 meV.

C. Parity analysis

Since all the investigated compounds possess inversion symmetry, a parity analysis⁴⁸ can be used to identify the Z_2 topological phases. There are eight time reversal invariant points in the rhombohedral Brillouin zone but only four points (Γ , F, L and Z; see Fig. 1 (D)) are inequivalent. Products of parity eigenvalues at these four momenta are given in Table II with and without spin-orbit coupling.

Table II, shows that product of parity eigenvalues in TlBiSe₂, TlBiTe₂, TlSbSe₂ and TlSbTe₂ changes at Γ as spin-orbit coupling is turned on, yielding a nontrivial topological invariant $Z_2 = 1$. The non-trivial topological

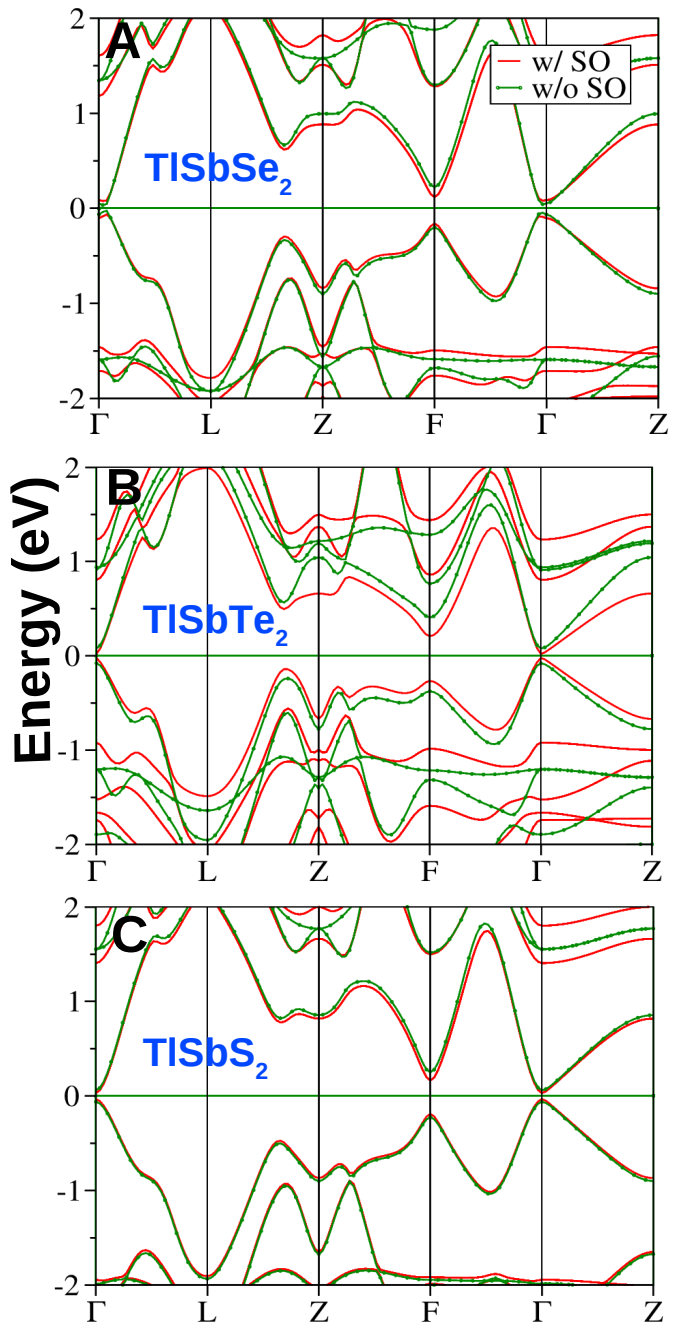


FIG. 2. Bulk band structures of rhombohedral (A) TlSbSe₂ (B) TlSbTe₂ (C) TlSbS₂ along high symmetry lines with (red lines) and without (green lines) spin-orbit coupling.

character of these compounds is thus due to band inversion at the Γ -point^{26,27,36}. On the other hand, there is no band-inversion for TlSbS₂ and TlBiS₂ at any of the time reversal invariant momenta, indicating that these compounds are topologically trivial.

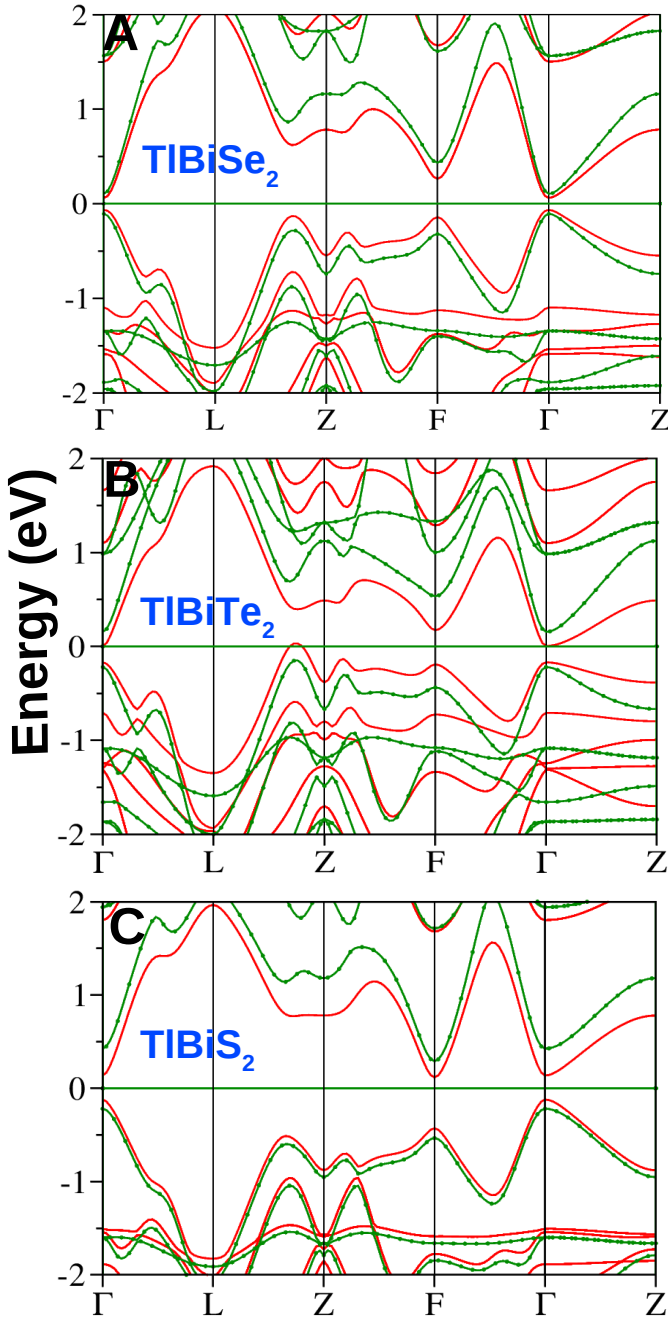


FIG. 3. Bulk band structures of rhombohedral (A) TlBiSe₂ (B) TlBiTe₂ (C) TlBiS₂ along high symmetry line with (red lines) and without (green lines) spin-orbit coupling.

IV. SURFACE ANALYSIS

A. Slab Structure and Relaxation

A hexagonal unit cell is used for all slab computations with atomic layers stacked in the z-direction. Since atoms along the z-direction are sequenced in the order Tl-Te(S, Se)-Bi(Sb)-Te(S, Se), there are four possible surface ter-

| Compound | Γ | $\times 1$ | L | $\times 3$ | F | $\times 3$ | Z | $\times 1$ | Z_2 |
|---------------------|----------|------------|-----|------------|-----|------------|-----|------------|-------|
| | wso | so | wso | so | wso | so | wso | so | |
| TlSbSe ₂ | + | - | + | + | + | + | + | + | 1 |
| TlSbTe ₂ | + | - | + | + | + | + | + | + | 1 |
| TlSbS ₂ | + | + | + | + | + | + | + | + | 0 |
| TlBiSe ₂ | + | - | + | + | + | + | + | + | 1 |
| TlBiTe ₂ | + | - | + | + | + | + | + | + | 1 |
| TlBiS ₂ | + | + | + | + | + | + | + | + | 0 |

TABLE II. Products of parity eigenvalues at the four inequivalent time-reversal invariant k-points in the six investigated compounds. 'wso' refers to without spin-orbit coupling and 'so' to with spin-orbit coupling.

minations, depending on which atom lies in the topmost layer. The bond length between Tl-Te is large ($d=350$ pm), whereas bond length between the Bi-Te is small ($d=318$ pm). Thus, out of the four possible surface terminations, we have used the one with Q (Se, Te and S) atom at the surface and Bi (Sb) under it in the second layer as this termination has a minimum number of dangling bonds²⁶. Optimized bulk parameters were used to construct slabs of different thicknesses. A symmetric 39 atomic layer slab of TlBiTe₂ and the associated surface Brillouin zone is shown in Fig. 4. Surface relaxation is known to play an important role^{36,37}, and accordingly, we have relaxed all atomic layers in the slabs used, although the relaxation effect is small as we move into the bulk.

B. TlSbQ₂ (Q=Se, Te and S)

The Q-atom terminated surface electronic structures of the three compounds are shown in Fig. 5 for different slab thicknesses together with the associated projected bulk bands (blue colored region). Figs. 5(A) and (B) show the surface band structure of TlSbSe₂ for slabs of 35 (thickness ≈ 6.4 nm) and 47 (thickness ≈ 8.6 nm) layers, respectively. In the 35 layer slab there is a band gap of 50 meV at the $\bar{\Gamma}$ -point. As the number of layers increases, the size of the gap decreases. For 47 layers, this gap is negligible and we get a clear Dirac-cone surface state in the bulk gap region. Moreover, around -0.8 eV we obtain a Rashba-type, trivial spin split surface state in both slabs³⁶. Fig. 5(C) shows results for a 47 layer TlSbTe₂ slab, which are similar to those for TlSbSe₂. Finally, TlSbS₂ does not display any surface state, which confirms its topologically trivial nature.

C. TlBiQ₂ (Q=Se, Te and S)

Similar to TlSbQ₂, TlBiQ₂ also shows thickness dependent slab electronic structure. Fig. 6 shows the surface band structure of TlBiSe₂. With a slab thickness of ≈ 6.3 nm we get a gapped surface state with a gap of 36 meV

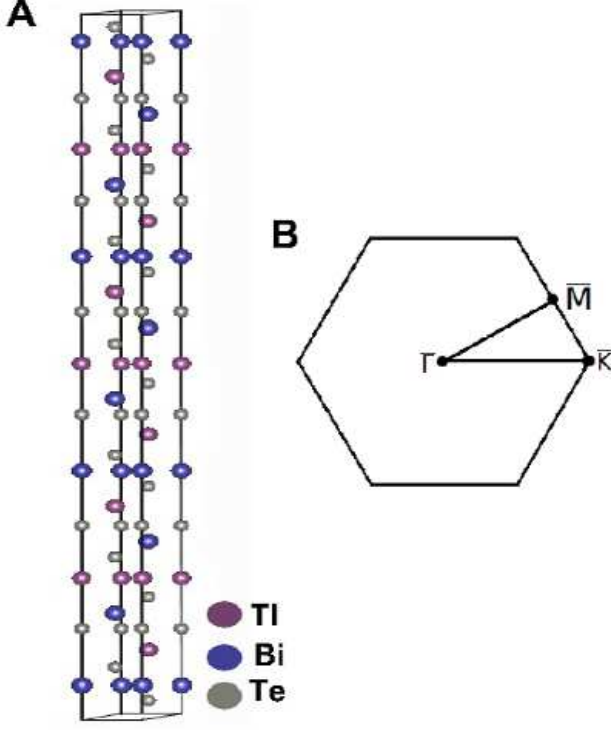


FIG. 4. (A) Structure of a 39 atomic layer slab of TlBiTe_2 stacked along the z -direction. (B) 2D Brillouin zone with three special k -points $\bar{\Gamma}$, \bar{M} and \bar{K} .

and as we increase slab thickness to ≈ 7.0 nm this gap reduces to 9 meV. The gap at small slab thickness arises due to interaction between the opposite faces of the slab. As we further increase the slab thickness to ≈ 8.7 nm and ≈ 10.9 nm we obtain a clear Dirac state with a negligible gap. At a critical thickness of ≈ 7.0 nm the Dirac point is isolated, i.e. no other states are at the energy of the Dirac point, which agrees with recent angle-resolved photo-emission spectroscopy (ARPES)^{29,30,28} measurements. The observed Dirac state for slabs thicker than 7.0 nm is surrounded by the surface bands, which is somewhat different from ARPES results and requires further study.

Fig 7(A) shows results for TlBiTe_2 , which exhibits a Dirac-like surface state in the bulk gap region at the thickness of ≈ 7.4 nm (39 layers). The Dirac point lies 0.1 eV below the Fermi energy in accord with ARPES studies²⁹. The electronic structure displays an indirect band gap near the $\bar{\Gamma}$ point with bulk conduction band minimum at the $\bar{\Gamma}$ -point and bulk valence band maxima along the $\bar{\Gamma} - \bar{M}$ and $\bar{\Gamma} - \bar{K}$ directions. The location of Dirac point in our calculation is close to experimental results, where Dirac point lies at 0.3 eV below the Fermi energy. Results for TlBiS_2 in Fig. 7(B) do not have any metallic surface state in the bulk gap region indicating its topologically trivial character.

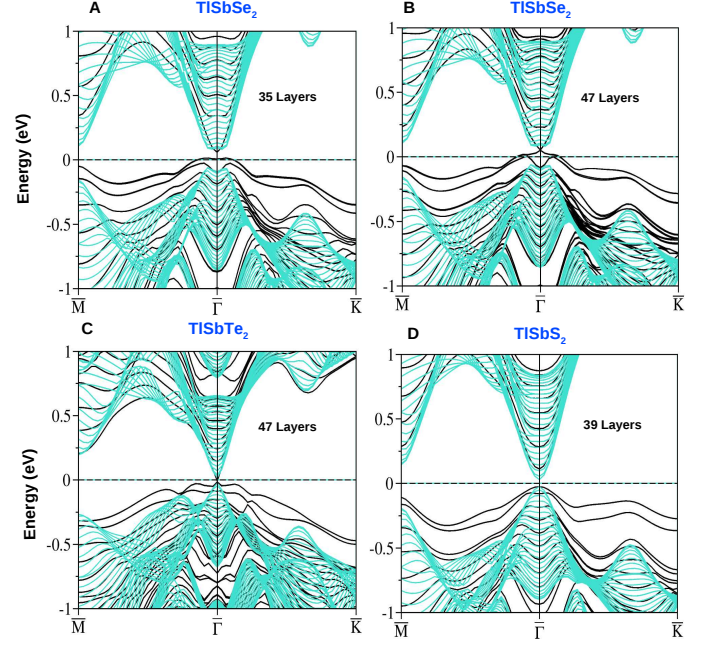


FIG. 5. Surface electronic structure of various slabs: (A) 35 layer (≈ 6.4 nm) TlSbSe_2 ; (B) 47 layer (≈ 8.6 nm) TlSbSe_2 ; (C) 47 layer (≈ 9.2 nm) TlSbTe_2 ; and (D) 39 layer (≈ 6.9 nm) TlSbS_2 , along high symmetry lines in the surface Brillouin zone. The bulk bands projected on the surface Brillouin zone are shown in blue color.

V. TOPOLOGICAL PHASE TRANSITION AND WEYL SEMIMETAL

A. $\text{TlBi}(\text{S}_{1-x}\text{Se}_x)_2$

The topological phase transition was observed in $\text{TlBi}(\text{S}_{1-x}\text{Se}_x)_2$ in which the S and Se atoms are disordered and inversion symmetry is preserved on the average with the inversion center at the (Se,S) site.³³ At the critical composition $x \sim 0.5$, the conduction and valence bands meet at the $\bar{\Gamma}$ point and form 3+1D Dirac-cone bulk states. The Dirac-cone states are doubly degenerate due to inversion and time-reversal symmetries. When the inversion symmetry is broken, the spin degeneracy can be lifted. Here we consider an ordered phase of TlBiSSe with layers in the order Tl-Se-Bi-S as shown in Fig. 8(E) and (F). The inversion symmetry is now seen to be broken as Se and S sites are no longer inversion centers. Our theoretical fully relaxed structure, which is rhombohedral, is found to be stable, indicating that the material should be possible to realize via molecular beam epitaxy (MBE) techniques. In the absence of inversion symmetry, parity analysis cannot be applied to delineate the topological nature, but adiabatic continuity arguments can be used. Accordingly, we start from the normal insulator with a large value of c/a and systematically reduce its value. During this process the system passes from

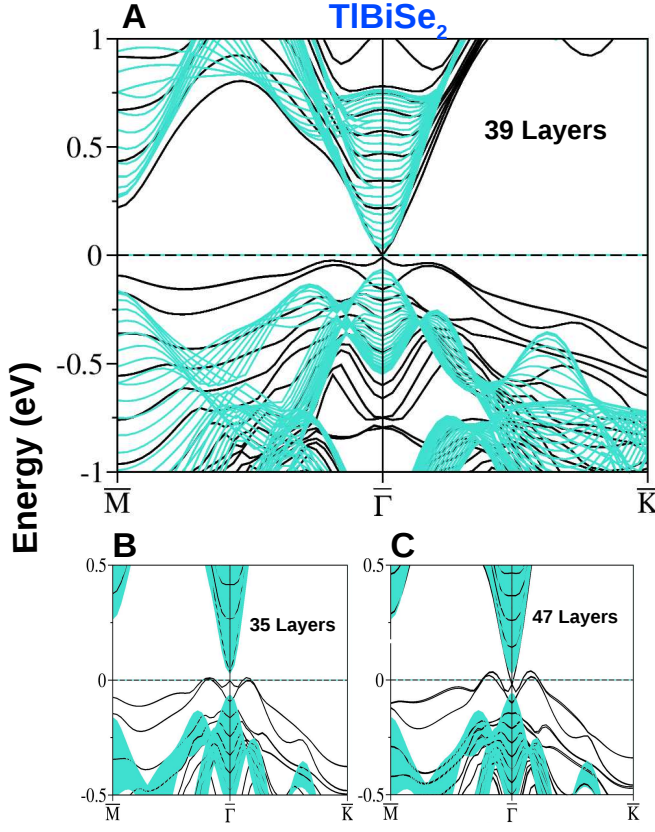


FIG. 6. Surface electronic structure of various slabs: (A) 39 layer (≈ 7.0 nm) TlBiSe_2 ; (B) 35 layer (≈ 6.3 nm) TlBiSe_2 ; and (C) 47 layer (≈ 8.7 nm) TlBiSe_2 , along high symmetry lines in the surface Brillouin zone. Projected bulk bands are shown in blue color.

normal to a topological insulator as shown in the Fig. 8(A). The band structure for the normal and topological phase through the critical point is shown in Figs. 8(B)-(D). The critical point occurs when the gap closes. At $c/a=4.98$, the band gap is 0.135 eV, and the bulk valence band has no s -character while the bulk conduction band possesses a finite s -character at Γ . These characteristic symmetries are the same as in TlBiSe_2 , indicating that the two compounds are adiabatically connected and are thus both topologically nontrivial. With increasing c/a value the gap decreases and becomes zero at the critical value $c/a=5.33$. Upon further increasing c/a , the bulk gap increases and becomes 0.129 eV at $c/a=5.58$ and the bulk valence and conduction bands swap their orbital character at the Γ -point. The system is now adiabatically connected to TlBiS_2 and is, therefore, topologically trivial.

Interestingly, at the topological critical point, the band gap at Γ remains finite with a value of 0.062 eV. However, the band gap closes along $\Gamma - L$ at $\vec{k}=(0.0, 0.0, 0.007)$. Thus, by breaking inversion symmetry, we obtain a nondegenerate spin-polarized bulk Dirac cone, instead of the doubly degenerate Dirac cone found in the Se/S

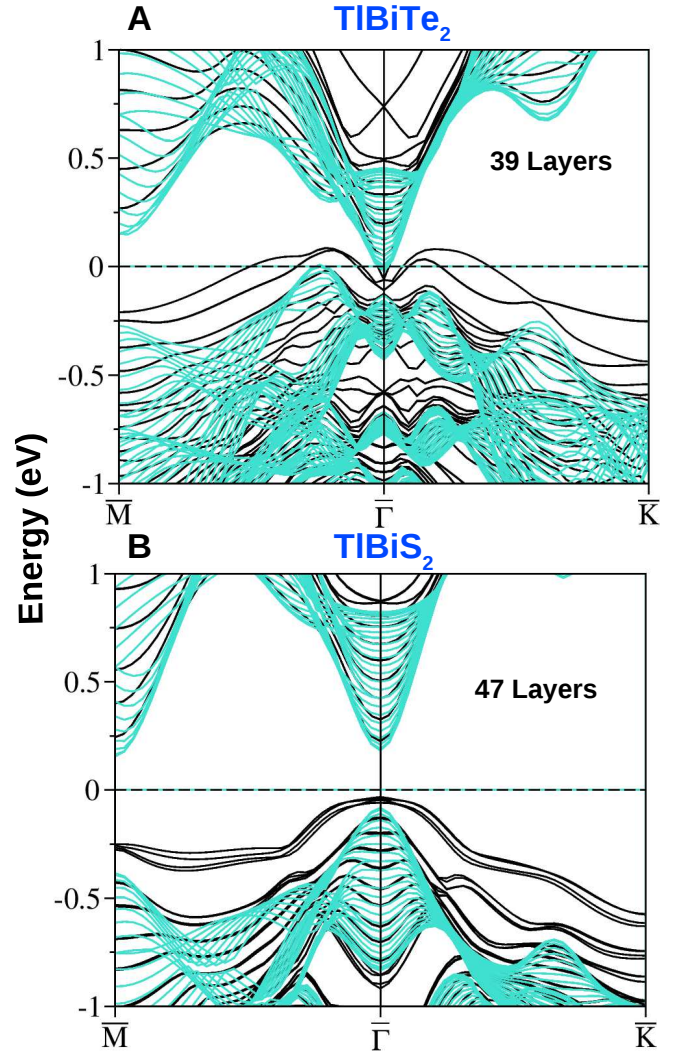


FIG. 7. Surface electronic structure of: (A) 39 layer (≈ 7.4 nm) TlBiTe_2 slab, and (B) 47 layer (≈ 8.6 nm) TlBiS_2 slab, along high symmetry lines in the surface Brillouin zone. The blue color shows projected bulk bands.

disordered $\text{TlBi}(\text{Se},\text{S})_2$. The bulk valence and conduction bands now touch each other and display linear dispersion, which can be described by a two component wave functions, i.e. by the Weyl equation. A Weyl semimetal is formed at the critical point with six Weyl points centered along $\Gamma - L$.⁴⁹ The detailed band structure is shown in Fig. 9.

B. $\text{TlBi}(\text{S}_{1-x}\text{Te}_x)_2$

Analysis of $\text{TlBi}(\text{S}_{1-x}\text{Te}_x)_2$ follows along the lines of that of $\text{TlBi}(\text{S}_{1-x}\text{Se}_x)_2$ in the preceding subsection, and therefore, we only make a few relevant remarks. Here again we take the critical point to be at $x=0.5$, and break the inversion symmetry by considering an ordered phase with layers in the sequence TI-Te-Bi-S , and com-

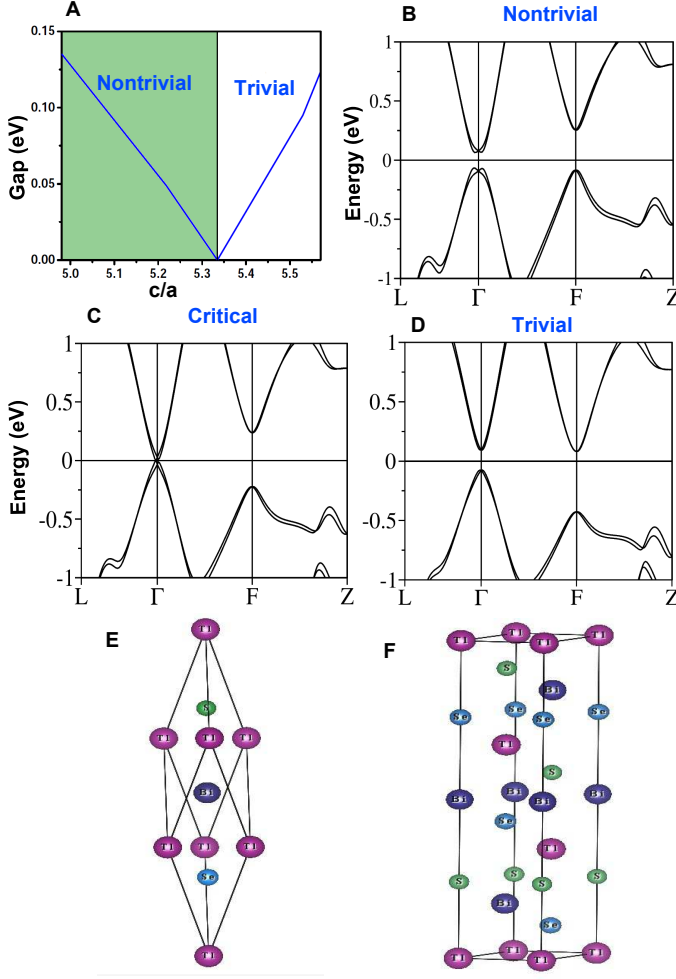


FIG. 8. (A) Phase diagram for the topological phase transition. The system is tuned from the normal to topological insulator by changing the c/a ratio. Panels (B)-(D) show the bulk band structure of TlBiSeS for $c/a=5.22$, $c/a=5.33$ and $c/a=5.58$, respectively. Primitive rhombohedral (E) and conventional hexagonal (F) crystal structure for TlBiSeS . The layered structure is with no inversion symmetry.

pute the band structure for a series of c/a values. The results, summarized in Fig. 10, show that at $c/a=4.93$ there is a direct band gap of 0.123 eV along $\Gamma - L$, although there is an indirect gap of $\approx 10\text{meV}$. At the critical value of $c/a=5.00$, the gap becomes zero along $\Gamma - L$ at $\vec{k} = (0.0, 0.0, 0.025)$, even though the gap remain finite at Γ with a value of 0.210 eV. With further increase in c/a , the gap reopens and becomes 0.221 eV at $c/a=5.57$. Adiabatic continuity arguments combined with the change in the orbital character of the bulk valence and conduction bands at the critical value of c/a then allow us to conclude the non-trivial to trivial insulator transition shown in Fig. 10(A). As to the Weyl semimetal phase, at the critical c/a value, $\text{TlBi}(\text{S}_{1-x}\text{Te}_x)_2$ displays six Weyl points along the $\Gamma - L$ direction at $\vec{k} = (0.0, 0.0, 0.025)$, although the spin split-

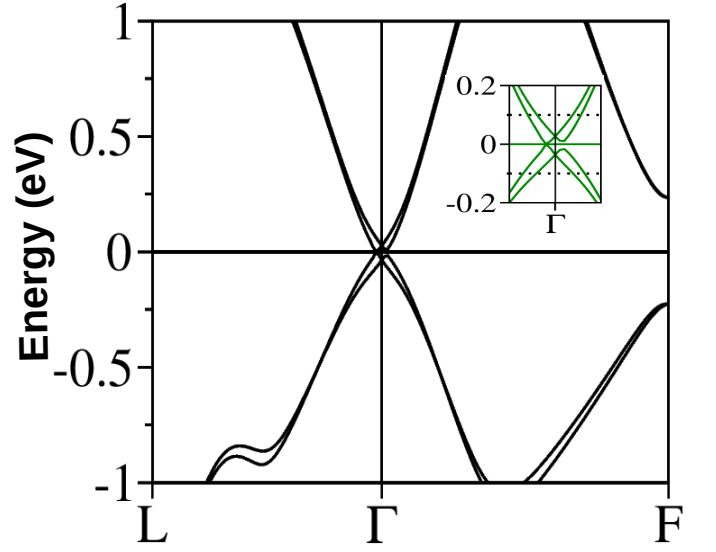


FIG. 9. Band dispersion at the critical point in $\text{TlBi}(\text{S}_{1-x}\text{Se}_x)_2$. Inset shows dispersion near the Γ -point.

ting is larger than in $\text{TlBi}(\text{S}_{1-x}\text{Se}_x)_2$.

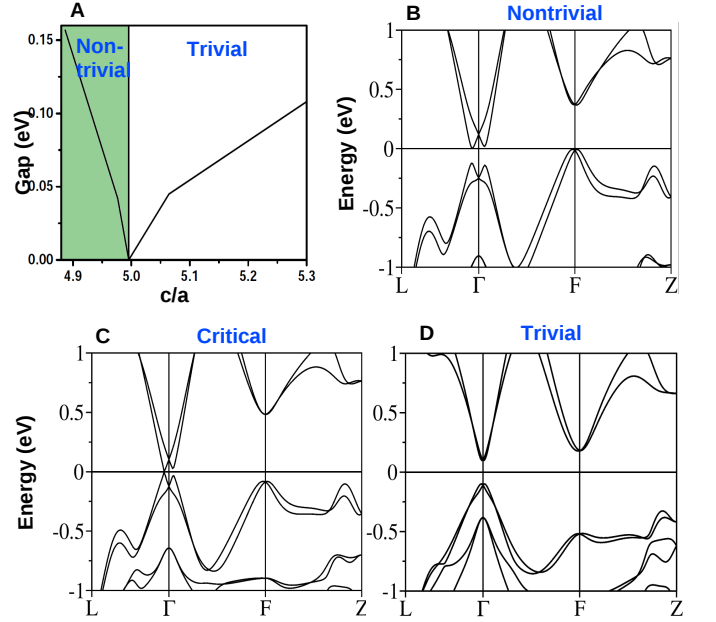


FIG. 10. (A) Phase diagram of topological phase transition in TlBiTeS . Panels (B)-(D) show the bulk band structure of TlBiTeS for $c/a=4.93$, $c/a=5.00$ and $c/a=5.57$, respectively

VI. CONCLUSIONS

We have carried out an *ab initio* study of bulk and surface electronic structures of six thallium based III-V-VI₂ ternary chalcogenides TMQ_2 , where M(Bi, Sb) and Q(S, Se or Te), with focus on delineating the topological na-

ture of these compounds. TlBiTe_2 is found to be a semi-metal with a band gap of -10 meV while the other five Tl-compounds are all small band gap semiconductors. Based on an analysis of parities of bulk band structures, we predict that TlSbSe_2 , TlSbTe_2 , TlBiSe_2 and TlBiTe_2 are non-trivial topological insulators with band inversion at the Γ -point, but TlSbS_2 and TlBiS_2 are trivial band insulators. Moreover, surface state computations show that the surface Dirac states lie in the gap region at the Γ -point in all four aforementioned topological compounds. Our predicted topological phases and the Γ -point centered Dirac-cone surface states are in substantial accord with available ARPES results. Electronic structures of slabs with different numbers of layers were computed in order to gain insight into thickness-dependent effects. The gap opens at the Dirac point for thin slabs and decreases with increasing thickness. Finally, we investigated $\text{TlBi}(\text{S}_{1-x}\text{Se}_x)_2$ and $\text{TlBi}(\text{S}_{1-x}\text{Te}_x)_2$ alloys for $x=0.5$ where the inversion symmetry was explicitly broken by using layers in the sequence Tl-Se(Te)-Bi-S and the c/a ratio was varied. Both alloys were found to undergo a topological transition at a critical value of c/a

at which the spin degeneracy of the Dirac states is lifted and a Weyl semimetal phase could be realized with six Weyl points in the bulk Brillouin zone located along the $\Gamma - L$ directions.

ACKNOWLEDGMENTS

We thank Diptiman Sen for helpful discussions. The work was supported by the Department of Science and Technology, New Delhi (India) through project SR/S2/CMP-0098/2010, the US Department of Energy, Office of Science, Basic Energy Sciences contract DE-FG02-07ER46352, and benefited from the allocation of supercomputer time at NERSC and Northeastern University's Advanced Scientific Computation Center (ASCC). MZH is supported by the Office of Basic Energy Sciences, U.S. Department of Energy grant No. DE-FG-02-05ER46200 and the A. P. Sloan Foundation Fellowship.

-
- ¹ X.-L. Qi and S.-C. Zhang, *Physics Today* **63**, 33 (2010).
 - ² M. Z. Hasan and C. L. Kane, *Rev. Mod. Phys.* **82**, 3045 (2010).
 - ³ J. E. Moore, *Nature(London)* **464**, 194 (2010).
 - ⁴ X.-L. Qi, T. L. Hughes, S. Raghu, and S.-C. Zhang, *Phys. Rev. Lett.* **102**, 187001 (2009).
 - ⁵ A. P. Schnyder, S. Ryu, A. Furusaki, and A. W. W. Ludwig, *Phys. Rev. B* **78**, 195125 (2008).
 - ⁶ F. Wilczek, *Nat. Phys.* **5**, 614 (2009).
 - ⁷ C. Nayak, S. H. Simon, A. Stern, M. Freedman, and S. Das Sarma, *Rev. Mod. Phys.* **80**, 1083 (2008).
 - ⁸ X. Wan, A. M. Turner, A. Vishwanath, and S. Y. Savrasov, *Phys. Rev. B* **83**, 205101 (2011).
 - ⁹ A. A. Burkov and L. Balents, *Phys. Rev. Lett.* **107**, 127205 (2011).
 - ¹⁰ G. B. Halász and L. Balents, *Phys. Rev. B* **85**, 035103 (2012).
 - ¹¹ S. Murakami, S. Iso, Y. Avishai, M. Onoda, and N. Nagaosa, *Phys. Rev. B* **76**, 205304 (2007).
 - ¹² K.-Y. Yang, Y.-M. Lu, and Y. Ran, *Phys. Rev. B* **84**, 075129 (2011).
 - ¹³ S.M. Young, S. Zaheer, J.C.Y. Teo, C.L. Kane, E.J. Mele, and A.M. Rappe, *Phys. Rev. Lett.* **108**, 140405 (2012).
 - ¹⁴ B. A. Bernevig, T. L. Hughes, and S.-C. Zhang, *Science* **314**, 1757 (2006).
 - ¹⁵ M. König, S. Wiedmann, C. Brüne, A. Roth, H. Buhmann, L. W. Molenkamp, X.-L. Qi, and S.-C. Zhang, *Science* **318**, 766 (2007).
 - ¹⁶ H. Zhang, C.-X. Liu, X.-L. Qi, X. Dai, Z. Fang, and S.-C. Zhang, *Nat. Phys.* **5**, 438 (2009).
 - ¹⁷ D. Hsieh, D. Qian, L. Wray, Y. Xia, Y. S. Hor, R. J. Cava, and M. Z. Hasan, *Nature* **452**, 970 (2008).
 - ¹⁸ Y. Xia, D. Qian, D. Hsieh, L. Wray, A. Pal, H. Lin, A. Bansil, D. Grauer, Y. S. Hor, R. J. Cava, and M. Z. Hasan, *Nat. Phys.* **5**, 398 (2009).
 - ¹⁹ J. G. Analytis, J.-H. Chu, Y. Chen, F. Corredor, R. D. McDonald, Z. X. Shen, and I. R. Fisher, *Phys. Rev. B* **81**, 205407 (2010).
 - ²⁰ K. Eto, Z. Ren, A. A. Taskin, K. Segawa, and Y. Ando, *Phys. Rev. B* **81**, 195309 (2010).
 - ²¹ N. P. Butch, K. Kirshenbaum, P. Syers, A. B. Sushkov, G. S. Jenkins, H. D. Drew, and J. Paglione, *Phys. Rev. B* **81**, 241301(R) (2010).
 - ²² A. Shitade, H. Katsura, J. Kunes, X.-L. Qi, S.-C. Zhang, and N. Nagaosa, *Phys. Rev. Lett.* **102**, 256403 (2009).
 - ²³ H. Lin, L. A. Wray, Y. Xia, S. Xu, S. Jia, R. J. Cava, A. Bansil, and M. Z. Hasan, *Nat. Mater.* **9**, 546 (2010).
 - ²⁴ S. Chadov, X. Qi, Jürgen Kübler, G. H. Fecher, C. Felser, and S. C. Zhang, *Nat. Mater.* **9**, 541 (2010).
 - ²⁵ M. Franz, *Nat. Mater.* **9**, 536 (2010).
 - ²⁶ H. Lin, R. S. Markiewicz, L. A. Wray, L. Fu, M. Z. Hasan, and A. Bansil, *Phys. Rev. Lett.* **105**, 036404 (2010).
 - ²⁷ B. Yan, C.-X. Liu, H.-J. Zhang, C.-Y. Yam, X.-L. Qi, T. Frauenheim, and S.-C. Zhang, *Europhys. Lett.* **90**, 37002 (2010).
 - ²⁸ K. Kuroda, M. Ye, A. Kimura, S. V. Eremeev, E. E. Krasovskii, E. V. Chulkov, Y. Ueda, K. Miyamoto, T. Okuda, K. Shimada, H. Namatame, and M. Taniguchi, *Phys. Rev. Lett.* **105**, 146801 (2010).
 - ²⁹ Y. L. Chen, Z. K. Liu, J. G. Analytis, J.-H. Chu, H. J. Zhang, B. H. Yan, S.-K. Mo, R. G. Moore, D. H. Lu, I. R. Fisher, S. C. Zhang, Z. Hussain, and Z.-X. Shen, *Phys. Rev. Lett.* **105**, 266401 (2010).
 - ³⁰ T. Sato, K. Segawa, H. Guo, K. Sugawara, S. Souma, T. Takahashi, and Y. Ando, *Phys. Rev. Lett.* **105**, 136802 (2010).
 - ³¹ R. A. Hein and E. M. Swiggard, *Phys. Rev. Lett.* **24**, 53 (1970).
 - ³² T. Sato, K. Segawa, K. Kosaka, S. Souma, K. Nakayama, K. Eto, T. Minami, Y. Ando, and T. Takahashi, *Nat. Phys.*

- 7**, 840 (2011).
- ³³ S.-Y. Xu, Y. Xia, L. A. Wray, S. Jia, F. Meier, J. H. Dil, J. Osterwalder, B. Slomski, A. Bansil, H. Lin, R. J. Cava, and M. Z. Hasan, *Science* **332**, 560 (2011).
 - ³⁴ H. Nielsen and M. Ninomiya, *Physics Letters B* **130**, 389 (1983).
 - ³⁵ H. B. Nielsen and M. Ninomiya, *Nucl. Phys.* **B185**, 20 (1981).
 - ³⁶ S. V. Eremeev, G. Bihlmayer, M. Vergniory, Y. M. Korablev, T. V. Menshikova, J. Henk, A. Ernst, and E. V. Chulkov, *Phys. Rev. B* **83**, 205129 (2011).
 - ³⁷ J. Chang, L. F. Register, S. K. Banerjee, and B. Sahu, *Phys. Rev. B* **83**, 235108 (2011).
 - ³⁸ P. Hohenberg and W. Kohn, *Phys. Rev.* **136**, B864 (1964).
 - ³⁹ G. Kresse and J. Furthmüller, *Phys. Rev. B* **54**, 11169 (1996).
 - ⁴⁰ G. Kresse and D. Joubert, *Phys. Rev. B* **59**, 1758 (1999).
 - ⁴¹ J. P. Perdew, K. Burke, and M. Ernzerhof, *Phys. Rev. Lett.* **77**, 3865 (1996).
 - ⁴² W. H. Press, B. P. Flannery, S. A. Teukolsky, and W. T. Vetterling, *Numerical recipes* (Cambridge University Press, New York, 1986).
 - ⁴³ E. F. Hockings and J. G. White, *Acta Crystallographica* **14**, 328 (1961).
 - ⁴⁴ O. Madelung, *Semiconductors: data handbook*, 3rd ed. (Springer-Verlag, Berlin, 2004).
 - ⁴⁵ K. Hoang and S. D. Mahanti, *Phys. Rev. B* **77**, 205107 (2008).
 - ⁴⁶ S. Satpathy, S. K. Mishra, and O. Jepsen, *Condensed Matter* **9**, 461 (1997).
 - ⁴⁷ R. Nesper, S. Wengert, A. Savin, and T. E. Fassler, *Angew. Chem. Int. Ed. Engl.* **36**, 1808 (1997).
 - ⁴⁸ L. Fu and C. L. Kane, *Phys. Rev. B* **76**, 045302 (2007).
 - ⁴⁹ A topologically protected Weyl semimetal phase can be realized by removing the rotation symmetry of the crystal. The gapless semimetal phase is then stable over a finite region of a tuning parameter.